# Excited State Dynamics in FMO Antenna Complexes from Photosynthetic Green Sulfur Bacteria: A Kinetic Model

**Simone I. E. Vulto,**[†] **Michiel A. de Baat,**[†] **Sieglinde Neerken,**[†] **Frank R. Nowak,**[†] **Herbert van Amerongen,**[‡] **Jan Amesz,**[†] **and Thijs J. Aartsma\*,**[†]

*Department of Biophysics, Huygens Laboratory, Leiden University, P.O. Box 9504, 2300 RA Leiden, The Netherlands, and Biophysics Department, Free University, De Boelelaan 1081, 1081 HV Amsterdam, The Netherlands*

*Received: December 10, 1998; In Final Form: April 22, 1999*

We have simulated the excited state dynamics of the FMO (Fenna−Matthews−Olson) bacteriochlorophyll *a*-protein complexes of the green sulfur bacteria *Chlorobium (C.) tepidum* and *Prosthecochloris (P.) aestuarii* at cryogenic temperature in terms of an exciton model. The simulation is based on the electronic structure, as described in previous publications (Louwe, R. J. W.; Vrieze, J.; Hoff, A. J.; Aartsma, T. J. *J. Phys. Chem.* **1997**, *101*, 11280. Vulto, S. I. E.; de Baat, M. A.; Louwe, R. J. W.; Permentier, H. P.; Neef, T.; Miller, M.; van Amerongen, H.; Aartsma, T. J. *J. Phys. Chem.* **1998**, *102*, 9577). Relaxation between exciton states is described by linear electron phonon coupling as a perturbation term in the Hamiltonian of the system. The simulation was compared with experimental data obtained by pump−probe measurements with various wavelengths of excitation. For *C. tepidum*, a quite good agreement was obtained between the calculated and measured dynamics. For *P. aestuarii*, the simulations are less satisfactory but they can be improved by including static disorder. We conclude that not only the steady-state optical spectra but also the excited-state dynamics in the FMO complex at low temperature can be described with a simple exciton model.

## Introduction

Previous papers from our laboratory concerned the simulation of the electronic structures of the Fenna−Matthews−Olson (FMO) pigment protein complexes from two species of green sulfur bacteria, *Prosthecochloris aestuarii*[1] and *Chlorobium tepidum.*[2] Using smaller dipolar interaction energies between the bacteriochlorophylls (BChls) than applied in earlier simulations,[3−5] the various steady-state optical spectra could be quite well described, with only a single set of parameters for each bacterium. A direct consequence of the model was that the interactions between BChls belonging to different subunits of the FMO trimer could be neglected. For both FMO complexes, BChl 3, numbered according to Fenna and Matthews,[6] was found to be the molecule with the lowest site energy. We recently extended the simulations by calculating the absorbance difference spectra of the singlet excited states.[7] These spectra were compared with experimental data, in particular with spectra measured at long delay times, i.e., when energy equilibration was complete, and with spectra taken immediately after excitation. This resulted again in good agreement between experiment and simulation, thus confirming the essential features and parameters of the exciton model proposed by Louwe et al.[1]

It may be concluded that significant progress has been made in solving the long-standing problem of simulating the optical spectra of the FMO complex. It is remarkable that this result was achieved with a rather simple model, with a minimal set of parameters. The major question that remains is to what extent this model can account for the excited state relaxation, as

measured for example in transient absorption measurements.[7−9] Under the assumption that the stationary states of the system are described by the exciton wave functions, the transitions between the exciton states can only be induced by vibronic coupling to phonons and localized vibrations. The FMO complex provides a unique system to study the effect of vibronic coupling on relaxation between exciton levels. First of all, our current understanding of the electronic spectrum of the FMO complex[1,2] provides a simple theoretical framework in which vibronic coupling can be incorporated in a straightforward way. Second, the exciton structure in the absorbance difference spectra provides a fingerprint, dependent on the wavelength of excitation and on time, by which theory and experiment can be compared. Such a study is not only a critical test for the exciton model of the FMO complex but more generally for modeling the excited state dynamics in a coupled pigment system, especially at low temperature when thermally induced processes can be neglected.

In the present communication, we shall address the time dependence of the absorbance difference spectra of the FMO complex at different wavelengths of excitation and discuss the possible mechanism of energy relaxation within a subunit at cryogenic temperature. Experimentally, these processes have been extensively studied by time-resolved[8−15] and hole-burning[16−18] spectroscopy, showing rapid downhill energy transfer within a subunit with time constants ranging from tens of femtoseconds to a few picoseconds. The mechanism of these processes is still uncertain, but it has been suggested that the energy relaxation within a subunit is phonon assisted[8,11,17] and that the rate of relaxation from a given exciton state is mainly determined by the number of levels that are lower in energy.[8] Further, it has been shown that the Förster mechanism for energy transfer does not apply.[9,19] On the basis of time-resolved absorbance difference measurements,[9] a kinetic model was

---

\* Corresponding author. Fax: 31-71 5275819. E-mail: aartsma@biophys.leidenuniv.nl.
† Leiden University.
‡ Free University.

proposed, in which the rate constants resulting from the fitted kinetics were included. It was concluded that energy transfer should be regarded in terms of an excitonically coupled system.[9,17]

The theory of exciton relaxation and methods of simulating corresponding experimental data have been described extensively.[20–23] Recently, several groups have applied such theories to simulations of the excited state dynamics in photosynthetic systems. Leegwater et al.[23] simulated the room-temperature dynamics within the reaction center of photosystem II, by comparing calculated rates of excited state relaxation with the result of transient absorption measurements. They assumed that the exciton−phonon interaction is fairly weak and therefore used this interaction as a perturbation parameter. In this way, Leegwater et al.[23] studied the energy relaxation towards thermal equilibrium. Similar methods have been recently applied to the LH2 complex of purple bacteria,[24] and to the FMO complex[25] of *C. tepidum*. In these studies too, it was assumed that exciton relaxation occurs by a coupling to the vibrations of the protein matrix and that this coupling is weak compared to the dipolar interactions between the BChls. Renger and May[25] introduced a so-called correlation radius of the protein vibrations to take into account a delocalized protein−pigment interaction.

In the present paper, we apply the method used by Leegwater et al.[23] to the FMO complexes of both *C. tepidum* and *P. aestuarii*. In addition to the electronic structures described previously,[1,2] the coupling of the phonons to the vibrational modes within the system was included to simulate the dynamics for both FMO complexes. For *C. tepidum*, this procedure resulted in a quite satisfactory description of the time-resolved absorbance difference spectra at various excitation wavelengths. For *P. aestuarii*, the agreement between simulation and experiment was somewhat less good. This may possibly be due to the exclusion of effects associated with static disorder. We conclude that a good description of the excited state dynamics in the FMO complexes can be obtained, with the exciton model proposed by Louwe et al.[1] Therefore, this model proves to be a consistent framework for the interpretation of a variety of experimental data and constitutes a faithful representation of the electronic structure of the FMO complex.

## Materials and Methods

**Experimental.** FMO complexes from *P. aestuarii* and *C. tepidum* were isolated as described by Francke and Amesz[26] and dissolved in 50 mM Tris/HCl and 200 mM sodium chloride (pH 8.3). To obtain a clear glass upon cooling, 66% (v/v) glycerol was added. The samples were contained in a 0.5 mm cuvette and adjusted to an absorbance of 0.5 at 809 nm at room temperature.

Time-resolved transient absorption measurements were performed with a home-built amplified dye laser system with continuum generation and optical multichannel analyzer (OMA) detection, operating at 10 Hz.[27,28] The time resolution was 300 fs. Wavelength-selective excitation pulses were obtained by passing the continuum pulse through an amplifying dye cell (pumped by a frequency-doubled, Q-switched Nd:YAG laser) and subsequently through a suitable interference filter with a bandwidth of 6−10 nm (Ferroperm, CVI). The dye LDS 821 (Exciton) was used for amplification. The probe beam was polarized at the magic angle with respect to the pump. At each delay, 3000−5000 spectra were recorded and averaged. Per pulse about 0.5% of the bacteriochlorophylls were excited; therefore, annihilation effects could be neglected. We corrected for the group velocity dispersion by applying a third-order

**TABLE 1: Electronic Structures for the FMO Complexes of *C. tepidum* and *P. aestuarii* Resulting from the Simulations Described in Refs 2 and 1, Respectively[a]**

| | *C. tepidum* | | | *P. aestuarii* | | |
|---|---|---|---|---|---|---|
| state | excited state energy (cm$^{-1}$) | dipole strength (D$^2$) | BChl | excited state energy (cm$^{-1}$) | dipole strength (D$^2$) | BChl |
| 1 | 12113 (*825.6*) | 48.9 | 3 | 12112 (*825.6*) | 46.7 | 3 |
| 2 | 12262 (*815.5*) | 121.0 | 4 | 12266 (*815.3*) | 151.5 | 1 |
| 3 | 12355 (*809.6*) | 79.5 | 1 | 12293 (*813.5*) | 57.2 | 4 |
| 4 | 12414 (*805.6*) | 92.3 | 5,6 | 12396 (*806.7*) | 89.3 | 6 |
| 5 | 12448 (*803.3*) | 59.8 | 7 | 12457 (*802.8*) | 90.7 | 7 |
| 6 | 12611 (*793.0*) | 27.6 | 5,6 | 12496 (*800.3*) | 11.7 | 2 |
| 7 | 12649 (*790.6*) | 52.2 | 2 | 12634 (*791.5*) | 35.5 | 5 |

$^a$ The exciton states are numbered in order of increasing energy, with the corresponding wavelengths in nm (italics) given in parentheses. The fourth and the seventh columns show the BChls with a major contribution to the corresponding exciton state. The BChls are numbered according to Fenna and Matthews.[6]

polynomial function which was obtained by measuring the dispersion in CS$_2$.[29,30]

For the fluorescence measurements, the sample was selectively excited with a home-built picosecond dye laser as described previously,[31] with an excitation bandwidth of 0.5 nm (fwhm). The fluorescence was detected by a spectrometer equipped with an OMA detector, with a spectral resolution of 0.1 nm. Both fluorescence and time-resolved absorbance difference measurements were performed at 10 K in a helium flow cryostat (Utreks-LSO, Estonia).

**Simulations.** *Absorbance Difference Spectra.* The electronic structure of a system can be described by its Hamiltonian, $\hat{H}_0$, which for interacting pigments can be formulated as follows:

$$\hat{H}_0 = \sum_j E_j |j\rangle\langle j| + \sum_{j<i} V_{ij}(|j\rangle\langle i| + |i\rangle\langle j|) \tag{1}$$

Here, $E_j$ is the site energy of pigment $j$ and $V_{ij}$ is the dipole−dipole interaction between the $i$th and $j$th BChl. Parameters for the description of the electronic structure of the FMO complexes from *P. aestuarii* and *C. tepidum* were taken from refs 1 and 2 and are summarized in Table 1. The exciton simulations were based on the following assumptions:[1] (i) only interactions within a single subunit are significant; (ii) the effective dipole strength in calculating the interaction energies is 28.7 D$^2$; (iii) BChl 3 (the numbering is that of Fenna and Matthews[6]) is taken to be the pigment with the lowest site energy. With the parameters from Table 1, it was possible to fully describe nearly all experimentally available steady-state optical spectra of both complexes.[1,2] To each transition a Gaussian band was assigned with a width of 80 cm$^{-1}$ at half-maximum to account for the inhomogeneous broadening. Lifetime (homogeneous) broadening effects were neglected to minimize the number of parameters.

The energy levels of the two-exciton states and the corresponding oscillator strengths were calculated as described in refs 7, 9, 13, and 32. Briefly, the absorbance difference spectrum for each state is given by

$$\Delta A(\lambda,k) = -\text{ABS}(\lambda) - \text{SE}(\lambda,k) + \text{ESA}(\lambda,k) \tag{2}$$

where $\Delta A(\lambda,k)$ denotes the absorbance difference spectrum for the $k$th state, $\text{ABS}(\lambda)$ the absorption spectrum of the ground state, $\text{SE}(\lambda,k)$ the stimulated emission from the $k$th exciton state, and $\text{ESA}(\lambda,k)$ the absorption spectrum of the transition from the $k$th state to the two-exciton state. It was assumed that the spectrum of the stimulated emission was equal to the absorption

Excited State Dynamics in FMO Antenna Complexes

*J. Phys. Chem. B, Vol. 103, No. 38, 1999* **8155**

spectrum for the *k*th state, i.e., the Stokes shift was neglected.[7] The explicit expressions for ABS($\lambda$), SE($\lambda$,*k*), and ESA($\lambda$,*k*) are given in eqs 4−6 of ref 13.

*Kinetic Model.* Energy transfer is described by the general master equation[20] or the equivalent stochastic Liouville approach.[21,33−35] All basic information needed to characterize the dynamics of the electronic transitions is contained in the density matrix. Since no vibrational coherences have been observed[36] and the electron−phonon coupling is weak,[17,18,37] the electron−phonon interaction in the FMO complex is expected to be smaller than the dipole−dipole interactions. In this case, the electron−phonon interaction can be treated as a perturbation. The Liouville−von Neumann equation of motion[21,23] describing the time evolution of the reduced density matrix $\rho^{\text{red}}(t)$, is then given by

$$\frac{\text{d}}{\text{d}t}\rho^{\text{red}}(t) = -i[\hat{H}_0, \rho^{\text{red}}] - \hat{\Gamma}\rho^{\text{red}}(t) \qquad (3)$$

where $\hat{H}_0$ is the Hamiltonian describing the system (eq 1) and $\hat{\Gamma}$ the decay (relaxation) operator.[23] This equation has been used extensively to describe the excited state dynamics in coupled molecular systems, as reviewed in refs 20, 21, and 38.

Accumulated photon echo experiments[37] have demonstrated that the dephasing time in the red edge of the absorption spectrum is longer than 100 ps at temperatures of <10 K. This value is representative of optical dephasing of state 1 in the exciton model in the absence of energy relaxation and intersubunit energy transfer. (Energy relaxation and intersubunit energy transfer are responsible for the shorter time constants observed in the photon echo decays). We assume that this >100 ps time constant is also representative for the pure dephasing of other states, since the dephasing rate is mainly determined by the protein (bath) dynamics. Therefore, it can be assumed that the dephasing times are much longer than the bath correlation times, and it has been pointed out in refs 23 and 24 that under these conditions the dynamics of populations and coherences are decoupled (Bloch model). Actually, the experiments are performed under conditions (10 K, time scale < 10 ps) were pure dephasing effects (represented by the off-diagonal elements of the density matrix) are negligible. Therefore, the excited state dynamics is governed by population relaxation, induced by vibronic coupling, and only the diagonal terms of the density matrix are relevant. In matrix form, we have for the diagonal elements

$$\frac{\text{d}}{\text{d}t}\rho^{\text{red}}_{kk}(t) = -\Gamma_{kk,ll}\rho^{\text{red}}_{ll}(t) \qquad (4)$$

with $\rho_{kk}(t)$ being the probabilities of finding a molecule in the *k*th exciton state at time *t*, and $\Gamma_{kk,ll}$ the population transfer rate from exciton state *k* to exciton state *l*. $\Gamma_{kk,ll}$ is given by[23]

$$\Gamma_{kk,ll} = 2\delta_{k,l}\sum_{j,m}\gamma(\omega_l - \omega_m)|\langle j|\psi_m\rangle|^2|\langle j|\psi_l\rangle|^2 -$$
$$2\sum_j\gamma(\omega_l - \omega_k)|\langle j|\psi_k\rangle|^2|\langle j|\psi_l\rangle|^2 \qquad (5)$$

where $\delta$ is the Kronecker delta, $\gamma(\omega)$ is the spectral density which describes the frequency-dependent coupling of the electronic states of the complex to its environment (the phonon bath), $|j\rangle$ denotes the wave function of the system with excitation on pigment *j*, $|\psi_k\rangle$ is the wave function of exciton state *k*, which consists of linear combinations of $|j\rangle$. Equation 5 shows that the energy transfer is determined by $|\langle j|\psi_m\rangle|^2|\langle j|\psi_l\rangle|^2$, the product of the probability densities of excitations on pigment *j* in states
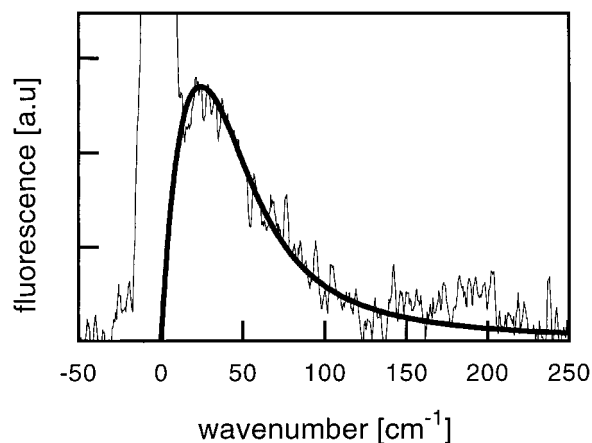


**Figure 1.** Fluorescence spectrum at 10 K of the FMO complex of *P. aestuarii* upon selective excitation at 827 nm. The thick solid line shows the profile for $\gamma(\omega)$, obtained with eq 6.

$|\psi_m\rangle$ and $|\psi_l\rangle$, respectively. Throughout the paper we will refer to this product as the overlap of probability densities. This implies that energy relaxation between two exciton states will be enhanced if their probability densities are overlapping significantly. The other important parameter of eq 5 is $\gamma(\omega)$, which accounts for energy relaxation through vibronic coupling of an exciton state with the phonon bath, a mechanism which has been evoked to explain kinetic data on the FMO complex.[8,17,37]

We have applied the above formalism to the excited state dynamics of the FMO complexes of *P. aestuarii* and *C. tepidum*. The electronic description of these systems[1,2] is summarized in the Hamiltonian, $\hat{H}_0$, given by eq 1. Diagonalization of the Hamiltonian, in combination with the data of the known X-ray structures,[6,39,40] provides the wave functions $|\psi_m\rangle$ of the exciton states in terms of linear combinations of localized molecular wave functions $|j\rangle$. To obtain a description for $\gamma(\omega)$, we have analyzed site-selective fluorescence measurements on the 825 nm band of the FMO complex of *P. aestuarii* at 10 K as shown in Figure 1. Fitting the shape of the phonon sideband gives an analytical description for $\gamma(\omega)$, assuming that the phonon sideband in the fluorescence spectrum is determined by linear electron−phonon coupling. Several functions for $\gamma(\omega)$ have been suggested in the literature.[23,25,41−43] Pullerits et al.[41] described the phonon sideband in a formal way, starting with a zero phonon line and adding a phonon sideband and vibrational bands. We found that this approach does not reproduce the long tail on the high-energy side of the phonon sideband, possibly because of the contribution of localized vibrational bands. Therefore, we chose to use an empirical approximation, using a combination of two functions to represent the phonon sideband:

$$\gamma(\omega) = \gamma_0 \begin{cases} \left(\dfrac{\Delta\omega}{2}\right)^2 \dfrac{1}{(\omega - \omega_c)^2 + \left(\dfrac{\Delta\omega}{2}\right)^2} & \omega \geq \omega_c \\ \dfrac{\omega}{\omega_c}\exp\left(1 - \dfrac{\omega}{\omega_c}\right) & \omega < \omega_c \end{cases} \qquad (6)$$

The Lorentzian function applies to the high-energy side of the phonon sideband ($\omega \geq \omega_c$), and the second equation describes the low-energy side of the function ($\omega < \omega_c$), as plotted in Figure 1. The maximum $\omega_c$ of the phonon sideband was at 24 cm$^{-1}$, in agreement with hole-burning measurements.[17] The value of $\Delta\omega$, the full width at half-maximum (fwhm) of the

**TABLE 2: Matrix $\Gamma_{kk,ll}$ Resulting from Eq 5 for Exciton Relaxation in *C. tepidum*[a]**

| exciton state | 7 | 6 | 5 | 4 | 3 | 2 | 1 |
|---|---|---|---|---|---|---|---|
| 7 | **13.77** | 0 | 0 | 0 | 0 | 0 | 0 |
| 6 | −12.21 | **6.56** | 0 | 0 | 0 | 0 | 0 |
| 5 | −0.07 | −1.82 | **23.33** | 0 | 0 | 0 | 0 |
| 4 | −0.26 | *−4.28* | −21.39 | **4.57** | 0 | 0 | 0 |
| 3 | −1.21 | −0.17 | −0.18 | −2.16 | **0.43** | 0 | 0 |
| 2 | −0.01 | −0.27 | −1.72 | −2.27 | −0.37 | **4.41** | 0 |
| 1 | −0.01 | −0.02 | −0.04 | −0.14 | −0.06 | −4.41 | 0 |

[a] The rate constants are given in $ps^{-1}$. The numbers refer to the numbers of the exciton states as defined in Table 1. The numbers in bold give the total decay rate for each state, and the numbers in italics show that extensive energy relaxation may also occur to non-neighboring states. $\gamma_0$ (see Materials and Methods) was adjusted to 111 $ps^{-1}$ to obtain the best fit of the time development of the absorption difference spectra shown in Figure 3.

Lorentzian, was taken to be 80 $cm^{-1}$. The only variable left was $\gamma_0$. This variable was used as a scaling parameter for adjusting the time axis of the simulated kinetics to match the one of the experimental data. We further assumed that the electron−phonon coupling is independent of the environment of the individual molecules. Therefore, we have taken $\gamma(\omega)$ to be the same for all states. In principle, $\gamma(\omega)$ is temperature dependent, but uphill energy transfer and temperature-dependent homogeneous dephasing are not significant under the conditions of our experiments. It has been shown by other groups that at higher temperatures (>50 K) this effect cannot be neglected anymore,[23,25] but this is beyond the scope of this communication. The decay matrix of eq 5 was calculated for both FMO complexes. Inserting eq 5 in eq 4 and solving the differential equations resulted in the relative population of the various exciton states with time.

**Results**

Although the X-ray structures[6,39,40] of the FMO complexes from *P. aestuarii* and *C. tepidum* are almost identical, this is not true for the absorption spectra; as noted earlier,[26] the spectrum of *P. aestuarii* has its maximum height at 815 nm, while the spectrum of *C. tepidum* has its maximum at 806 nm. These differences are also reflected in the simulated electronic structures,[1,2] as shown in Table 1. According to these simulations, in *P. aestuarii* the 815 nm band in the absorption spectrum results from two exciton states, 2 and 3 (mainly BChls 1 and 4), whereas in *C. tepidum* only state 2 (mainly BChl 4) is contributing to the band near 815 nm.

Using the method described in the previous section, we have simulated for both FMO complexes the absorbance difference spectra for excitation in each of the seven exciton states.[7] In almost all cases, the spectra showed a dominant bleaching at the wavelength of maximum absorption indicated for each state in Table 1. As discussed in the previous section, the dynamics of these excited states can be calculated by means of eq 5. This equation gives the matrix $\Gamma_{kk,ll}$ with the rate constants for phonon-assisted relaxation between exciton states. For *C. tepidum* the result is shown in Table 2. The only adjustable parameter for $\Gamma_{kk,ll}$ was $\gamma_0$, as mentioned before. This parameter was chosen to set the time axis of the simulation to obtain the best agreement between the time development of experimental and simulated difference spectra. It should be remarked that the results allow some conclusions that are independent of $\gamma_0$. First of all, it becomes clear that exciton states preferably relax stepwise downhill through the exciton manifold, since relaxation occurs mainly between two adjacent energy levels (see also ref
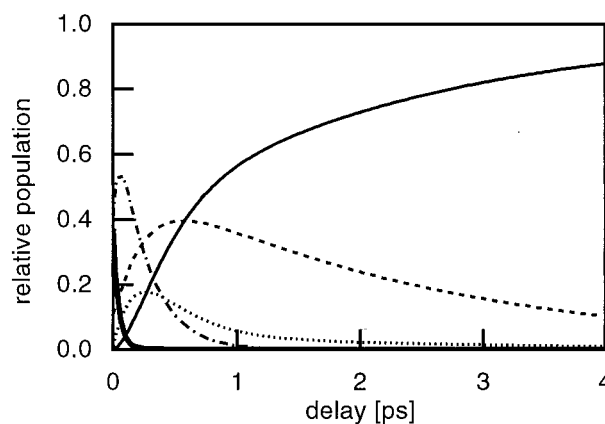


**Figure 2.** Population diagram of the various exciton states for the FMO complex of *C. tepidum* upon excitation at 800 nm: state 1 (solid); state 2 (dotted); state 3 (dashed); state 4 (dot−dashed); state 5 (thick solid line). The numbers of the states correspond to those of Table 1. The initial populations were calculated from the spectral distribution of the excitation pulse and the simulated absorption spectrum.[7] States 6 and 7 are not shown because they are hardly populated. $\gamma_0$ was adjusted to 111 $ps^{-1}$ to obtain an optimal simulation of the spectra of Figure 3.

25). Moreover, it is not merely the number of levels that are lower in energy that determines the rate of relaxation from a given exciton state. These rates are given by the bold numbers in the table, and it can be seen that state 3, with a decay constant of 2.4 ps, is the second most stable state (next to the lowest energy state 1, of which the lifetime is determined by the fluorescence lifetime or by the rate of energy transfer between subunits). All other states have decay constants of less than 1 ps, with states 5 and 7 as the most short-lived ones, with lifetimes of 43 and 73 fs, respectively. Thus, from Table 2 it can be immediately seen that these states, which show a maximum bleaching at 803 and 792 nm upon excitation,[2,7] cannot be detected with the time resolution of the experiments. Important factors determining the relaxation rates to lower energy levels are the difference in energy between two levels and the overlap of the probability density distribution of two exciton states, according to eq 5. The overlap reflects the condition that some BChls must contribute significantly to the exciton wave function of both states involved. The very high rate of relaxation from state 5 to state 4 is enhanced by a high value of $\gamma(\omega)$, due to the relatively small difference in energy between these states (Table 1), as can be seen from Figure 1 and eq 6. Another important factor, however, is the large contribution of the same BChls (5, 6, and 7) to both exciton states.[2] Conversely, the long lifetime of state 3 is due to the relatively large difference in energy with state 2, corresponding to a lower value of $\gamma(\omega)$, and the small couplings of BChl 1 with BChls 3 and 4, resulting in almost negligible overlap of the probability density of state 3 with that of states 1 and 2, respectively.

It is of interest to compare our exciton state lifetimes with those of Buck et al.[9] The fastest components (43 and 73 fs), which occur near 803 and 792 nm, were not resolved in their experiments. The lifetime of state 6 (150 fs, at 793 nm) corresponds to the 170 fs component at 795 nm. No clear evidence is seen in the experimental spectra of Buck et al.[9] for the roughly 200 fs decays of states 4 and 2, which should be visible in the range 805−815 nm. The 2.4 ps decay of state 3, however, is clearly observed with a maximum bleaching at 810 nm.

Figure 2 shows the relative populations of the various exciton states in time, upon excitation at 800 nm, as calculated from
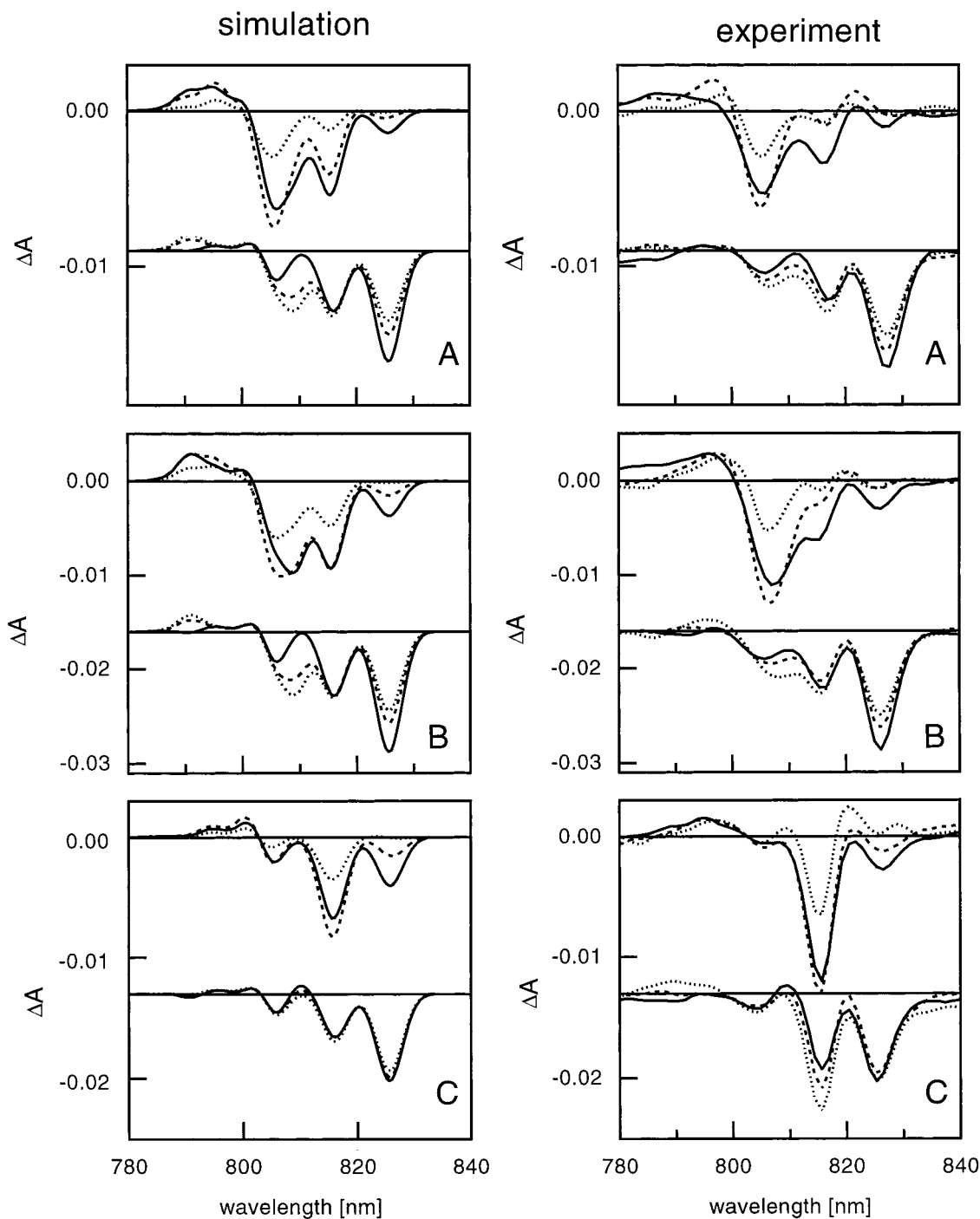
Excited State Dynamics in FMO Antenna Complexes

*J. Phys. Chem. B, Vol. 103, No. 38, 1999* **8157**

**Figure 3.** Calculated (left) and experimental (right) absorbance difference spectra for the FMO complex of *C. tepidum*, measured at 10 K. (A) Excitation at 800 nm, with an instrument response function of 300 fs (fwhm) and a bandwidth of ~10 nm. Spectra were taken at 60 (dotted), 260 (dashed), and 460 fs (solid) with respect to the maximum of the excitation pulse. Spectra at delays of 1.2 (dotted), 1.7 (dashed) and 3.9 ps (solid) are displaced downward. (B) Excitation at 807 nm, taken at 0 (dotted), 200 (dashed), and 400 fs (solid) delay. Spectra at delays of 0.8 (dotted), 1.7 (dashed), and 3.9 ps (solid) are shifted as indicated. (C) Excitation at 817 nm, taken at 60 (dotted), 260 (dashed), and 460 fs (solid). Spectra at delays of 1.0 (dotted), 1.8 (dashed), and 2.8 ps (solid) are displaced downward.

Table 2 using eq 4. The initial conditions were calculated from the simulated absorption bands of the various exciton states in the absorption spectrum and from the spectral distribution of the excitation pulse.[7] Note that initially the population is almost evenly distributed over states 4 and 5. These states depopulate rapidly with a concomitant population increase of states 2 and 3. This is followed by a decay of state 2, and within less than 1 ps after excitation, states 3 and 1 become the dominant ones. The population of state 1 shows a more or less biphasic growth. During the first picosecond, its growth is mainly determined

by the energy transfer from state 2 to 1, but later on, it is the slow decay of state 3 to state 2 that is the bottleneck in populating state 1, whose population reaches a value of 0.87 after 4 ps.

Figure 3 compares the simulated and experimental difference spectra obtained with various wavelengths of excitation. Figure 4 shows the kinetics that can be derived from the spectra in Figure 3 with excitation at 800 nm. An instrument response function of 300 fs (fwhm) was used for the calculation. $\gamma_0$ was taken the same as in Table 2 and Figure 2. Experimental data
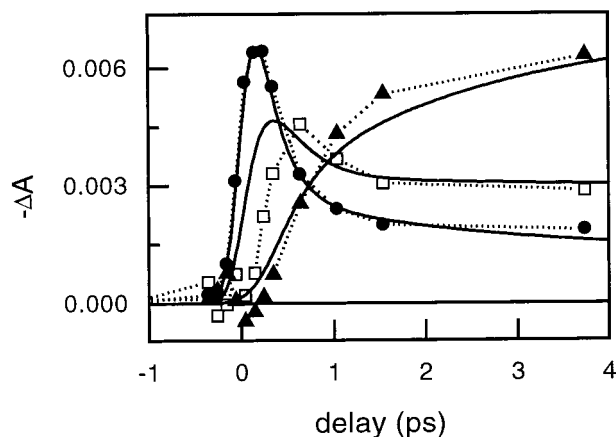
**Figure 4.** Calculated (solid) and experimental (dotted) kinetics for the FMO complex of *C. tepidum*, measured at 10 K, upon excitation at 800 nm, probed at 806 (dots), 815 (squares), and 825 (triangles) nm. The kinetic data are derived from the time-resolved spectra of Figure 3.

are shown on the right. For excitation at 800 nm (Figures 3A and 4), the time-dependent behavior could be nicely simulated for all absorption bands. The position of the negative band near 805−810 nm is well reproduced, too. Initially the bleaching is maximal at 805 nm, reflecting the population of states 4 and 5. State 5 rapidly depopulates, and this is observed as a red shift of the maximum from 805 to 806 nm at 400 fs delay and to 809 nm at 1 ps delay. In agreement with the experiment, at longer delays, the band shifts back to 806 nm, due to population of states 2 and 1. The maximum of the 825 nm band does not change with time, since we deal with a single exciton state, state 1, at this wavelength.[7] Similar features are observed upon 807 nm excitation. The shift in the 805−810 nm region is even more obvious. The amplitude of the 815 nm band is somewhat overestimated in the simulations, especially at early times both for excitation at 800 and at 807 nm. At longer times, however, a quite satisfactory agreement between experiment and simulation is obtained, and the spectra are essentially independent of the wavelength of excitation. Upon excitation at 817 nm, the amplitude of the 815 nm band is relatively large in the experimental spectra, compared with excitation at 800 and 807 nm. This phenomenon, for which we have no ready explanation, was noted earlier.[7]

For the FMO complex of *P. aestuarii*, the simulated population dynamics upon excitation at 806 nm are shown in Figure 5A. Initially states 4 and 5 are mainly populated. These states rapidly decay while energy is transferred to states 1, 2, and 3. State 3 is only briefly populated. State 2 is populated rapidly, and after a short time almost the entire population is in this state, which then slowly relaxes to state 1. These results are a direct consequence of the choice of site energies.[1] However, they are not in agreement with the experiments, which show that already more than 50% of the population is in state 1 after 1 ps (Figure 6 and refs 7 and 8). From the eigenvectors,[1] it follows that state 2 has a main contribution of BChl 1 and hardly any contribution of BChl 3, while state 1 involves mainly BChl 3 and hardly any BChl 1. Other BChls do not contribute much either to the overlap of probability densities between states 2 and 1. The simulated difference spectra are shown in Figure 6A, experimental ones in Figure 6C. It is immediately apparent that in the simulated spectra the 815 nm band is too pronounced due to the high population of state 2 and that the rise of the 825 nm band is much too slow in comparison to the experimental data.
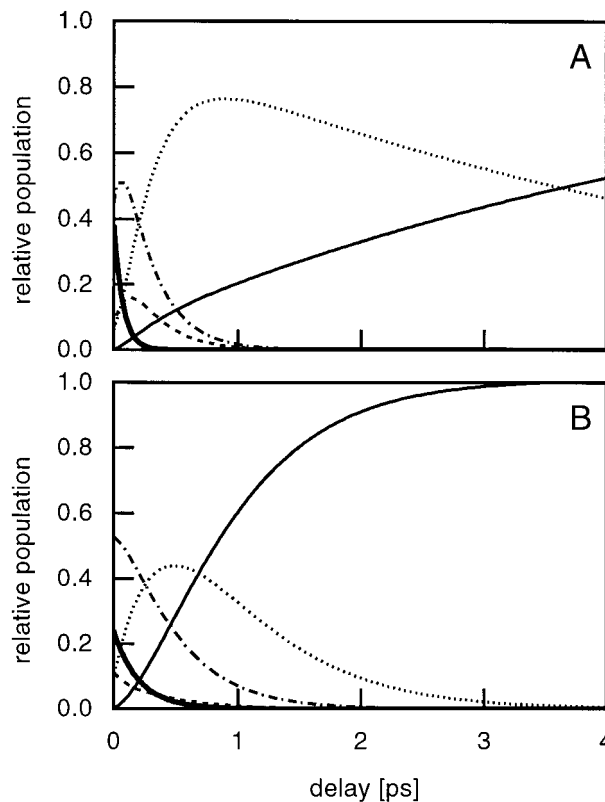


**Figure 5.** Population diagram of the various exciton levels for the FMO complex of *P. aestuarii*: state 1 (solid); state 2 (dotted); state 3 (dashed); state 4 (dot−dashed) and state 5 (thick solid line) upon excitation at 806 nm. States 6 and 7 are not populated at this excitation wavelength. The numbers of the levels correspond to those of Table 1. (A) Parameters for the exciton calculations were taken from ref 1. (B) Modified parameters taken from Tables 3 and 4. $\gamma_0$ was set at 87.5 ps$^{-1}$ for both simulations.

Because of the above discrepancies, we have tried to improve the exciton model. For *C. tepidum* (Figure 2), state 2 does not become strongly populated and state 1 becomes populated more rapidly, so a logical adjustment would be a choice of site energies to values more similar to those for *C. tepidum* (Tables 2, 3). This choice required in particular an adjustment of the site energies of BChls 1 and 4 (Table 3, second column). The steady-state spectra (absorption, linear dichroism (LD), triplet minus singlet (T−S), LD(T−S)) could be fitted equally well with a new set of parameters (Tables 3 and 4) as with the old ones, but the simulation for the circular dichroism (CD) spectrum deteriorated, and in particular the negative peak at 818 nm obtained in the earlier simulation[1] disappeared (not shown). The simulated absorbance difference spectra fitted the experimental ones as well as did the earlier calculated spectra.[7]

The rate constants for this amended model are shown in Table 5, while the populations of the exciton levels upon excitation at 806 nm are shown in Figure 5B. As for *C. tepidum,* the exciton states are seen to preferably relax stepwise. The shortest lifetime of 82 fs is found for state 7, in agreement with kinetic measurements,[8] and the longest lifetime is 630 fs for state 2. The latter differs from kinetic measurements[8] where components of 1.7 and 5.5 ps are observed with a maximum amplitude around 815 nm. (Note that the 37 ps component found in the kinetic measurements[8] is attributed to energy transfer between subunits). As in Figure 5A, initially mainly states 4 and 5 are populated, but they decay somewhat slower now. State 3 becomes hardly populated because of its short lifetime. The relaxation from state 2 to state 1 has considerably accelerated,
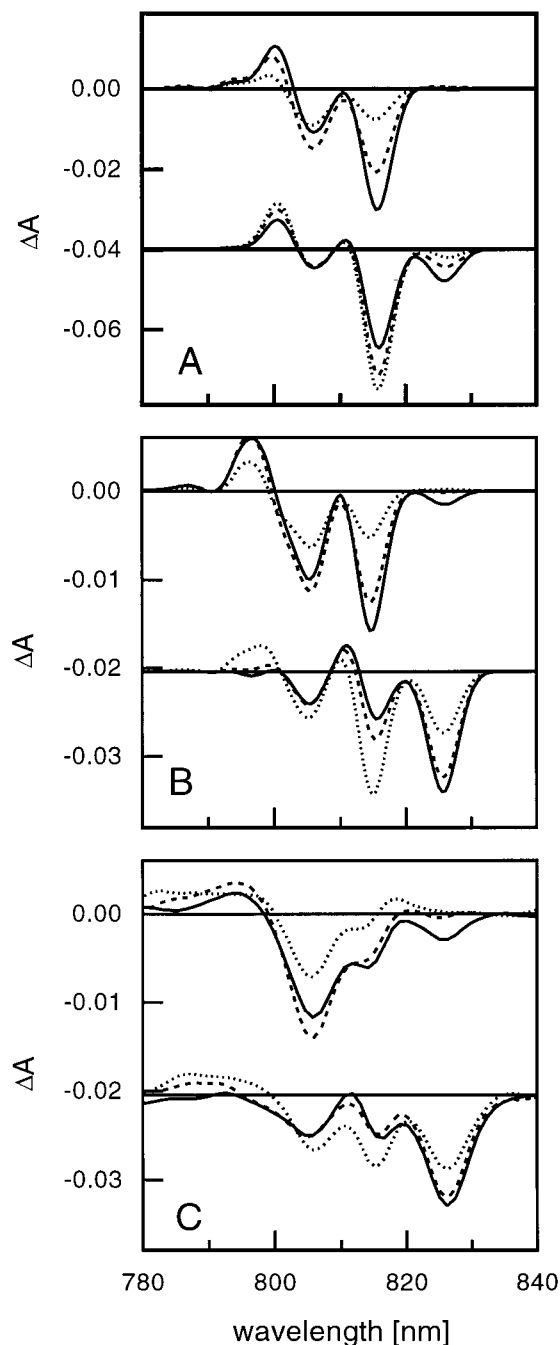
Excited State Dynamics in FMO Antenna Complexes

*J. Phys. Chem. B, Vol. 103, No. 38, 1999* **8159**



**Figure 6.** (A and B) Calculated and (C) experimental time-resolved absorbance difference spectra of the FMO complex from *P. aestuarii* at 10 K. (A) Calculated with the model of Louwe et al.[1] and (B) with the "new" parameters (see Tables 3 and 4). Excitation at 806 nm, taken at 0 (dotted), 200 (dashed). and 400 fs (solid) delay. Spectra at delays of 1.0 (dotted), 2.0 (dashed), and 3.9 ps (solid) are shifted downward.

due to the change of the site energies of BChls 1 and 4, since state 2 is now mainly associated with BChl 4, as in *C. tepidum*.[2]

When comparing the calculated difference spectra for *P. aestuarii* upon excitation at 806 nm with the experimental ones (Figure 6B,C), it is seen that at early times the correspondence between the simulated and experimental spectra is still not fully satisfactory. At 805 nm, the dynamics and amplitudes are quite well reproduced, but the peak at 815 nm in the simulations is too pronounced and decays too rapidly. However, the shift of the maximum of this band from 814 to 815 nm, due to relaxation from state 2 to 1, is well reproduced. The spectra at delays longer than 1 ps were nicely simulated. For excitation at 800 or 814

**TABLE 3: Site Energies Used for the Exciton Calculations for the FMO Complex of *P. aestuarii* as Used by Louwe et al.[1] (Right-Hand Column) and in This Work (Left); See Text[a]**

| | site energies (cm$^{-1}$) | | |
| | *P. aestuarii* | | |
| BChl no. | this work | ref 1 | *C. tepidum* (ref 2) |
|---|---|---|---|
| 1 | 12355 | 12320 | 12400 |
| 2 | 12510 | 12435 | 12600 |
| 3 | 12130 | 12130 | 12140 |
| 4 | 12300 | 12320 | 12280 |
| 5 | 12515 | 12570 | 12500 |
| 6 | 12480 | 12450 | 12500 |
| 7 | 12475 | 12430 | 12430 |

[a] For comparison, the site energies used for *C. tepidum* are given as well. The BChls are numbered according to Fenna and Matthews.[6]

**TABLE 4: Excited State Energies (cm$^{-1}$) and Dipole Strengths for the FMO complex of *P. aestuarii* Obtained from the Simulations Using the Site Energies Given in Table 3[a]**

| | | this work | | |
| state | excited state energies (cm$^{-1}$) (ref 1) | excited state energies (cm$^{-1}$) | dipole strength (D$^2$) | BChl |
|---|---|---|---|---|
| 1 | 12112 (*825.6*) | 12111 (*825.7*) | 49.7 | 3 |
| 2 | 12266 (*815.3*) | 12278 (*814.5*) | 138.8 | 4 |
| 3 | 12293 (*813.5*) | 12312 (*812.2*) | 60.6 | 1 |
| 4 | 12396 (*806.7*) | 12410 (*805.8*) | 100.3 | 6 |
| 5 | 12457 (*802.8*) | 12488 (*800.8*) | 71.1 | 7 |
| 6 | 12496 (*800.3*) | 12556 (*796.4*) | 26.7 | 2 |
| 7 | 12634 (*791.5*) | 12610 (*793.0*) | 34.6 | 5 |

[a] In parentheses, the corresponding wavelengths in nm. The BChls with a contribution higher than 60% to a particular state are identified (last column).

**TABLE 5: Matrix $\Gamma_{kk,ll}$ Resulting from Eq 5 for Exciton Relaxation in *P. aestuarii* Based on the Parameter Sets of Tables 3 and 4[a]**

| exciton state | 7 | 6 | 5 | 4 | 3 | 2 | 1 |
|---|---|---|---|---|---|---|---|
| 7 | **12.17** | 0 | 0 | 0 | 0 | 0 | 0 |
| 6 | −5.63 | **3.91** | 0 | 0 | 0 | 0 | 0 |
| 5 | *−3.31* | −1.97 | **5.37** | 0 | 0 | 0 | 0 |
| 4 | *−2.91* | −0.41 | −4.53 | **2.64** | 0 | 0 | 0 |
| 3 | −0.08 | *−1.44* | −0.07 | −0.64 | **7.69** | 0 | 0 |
| 2 | −0.23 | −0.08 | −0.76 | *−1.94* | −7.53 | **1.58** | 0 |
| 1 | −0.01 | −0.01 | −0.01 | −0.06 | −0.16 | −1.58 | 0 |

[a] The rate constants are given in ps$^{-1}$. The numbers refer to the numbers of the exciton states as defined in Table 1. The numbers in bold give the total decay rate of each state, and the numbers in italics show when significant energy relaxation occurs to non-neighboring states.

nm, the same features were observed. The experimentally observed components of 1.7 and 5.5 ps,[8] which can also be seen in the difference spectra of Figure 6 and of ref 7, are not found in the simulation. Within the present model this situation can only be improved by a change of $\gamma_0$ at the expense of the fit at shorter times.

## Discussion

The results shown in Figures 2 and 3 show that our kinetic model describes the dynamics of the FMO complex of *C. tepidum* quite well. This is the more remarkable because only one adjustable parameter ($\gamma_0$) was used in our simulations. All the other parameters were either the same as used in our earlier simulations or they were directly obtained from the site-selective
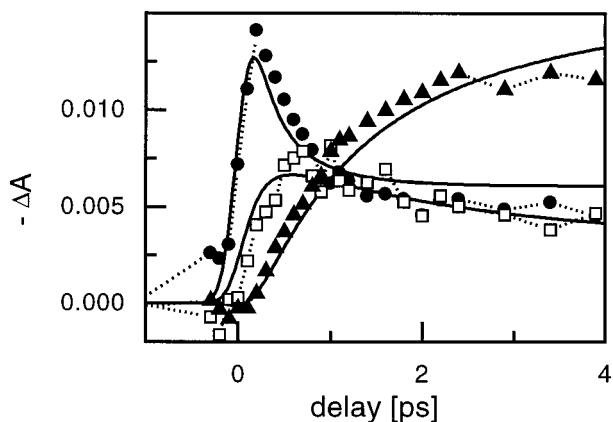
**Figure 7.** Calculated (solid) and experimental (dotted) kinetics for the FMO complex of *P. aestuarii*, measured at 10 K, upon excitation at 806 nm, probed at 806 (dots), 815 (squares), and 825 (triangles) nm. The kinetic data are derived from the time-resolved spectra of Figure 6C. The calculations are performed using the model of Louwe et al.,[1] including static disorder. It should be noted that the amplitude of the 815 nm band still remains somewhat too high in the simulation with respect to the 800 and 825 nm band. Therefore, the simulated kinetics are scaled in amplitude to the measured ones to emphasize the improvement of the kinetic behavior by including static disorder with respect to the simulations of parts A and B of Figure 6.

fluorescence spectrum of Figure 1. The results obtained with the FMO complex from *P. aestuarii* were clearly less satisfactory. This was true even when the site energies of the BChls had been adjusted to obtain a better fit of the population dynamics of states 1 and 2, compared to the model of Louwe et al.[1] The reason for the less satisfactory fit of *P. aestuarii* compared to *C. tepidum* is not clear, but it may be recalled that the same was found to be true for the steady-state optical spectra.[2]

We have also tested the assumption that BChls 2 and 6 are the lowest energy pigments, with the parameters described by Louwe et al.,[1] but as in the simulations of the optical spectra,[1] the correspondence of the calculated dynamics with the experimental data was far worse than when BChl 3 was taken as the lowest energy pigment.

With the parameters of Louwe et al.,[1] significant discrepancies were observed between the simulated and measured kinetics of the FMO complex from *P. aestuarii*. Some of these could be overcome by adjusting the relative site energies of mainly BChls 1 and 4. However, with the alternative set of parameters, the experimentally observed 1.7 ps component[8] is not reproduced. Apparently, the order of site energies of BChls 1 and 4 is critical. It is important to note that in both parameter sets for *P. aestuarii* the difference in site energies of BChls 1 and 4 is less than the inhomogeneous broadening, or static disorder. This implies that two types of FMO complexes may exist, which are distinguished by the relative order of the site energies of BChls 1 and 4. State 2, the second-lowest exciton state, is then dominated by either the contribution of BChl 1 or that of BChl 4, depending on which of these BChls has the lower site energy. The relatively slow component (1.7 ps) observed in the relaxation kinetics of the 815 nm band in *P. aestuarii* may then be attributed to a fraction of FMO complexes in which BChl 1 has a lower site energy than BChl 4. We have tested the effect of static disorder by a Monte Carlo simulation[44] of the optical spectra and relaxation kinetics of *P. aestuarii*. A distribution of time constants was found centered around the values obtained in the simulations, which are shown for each model in Figure 5. In particular, for state 2, a distinct separation of time constants was obtained in two time domains, one around a few hundred
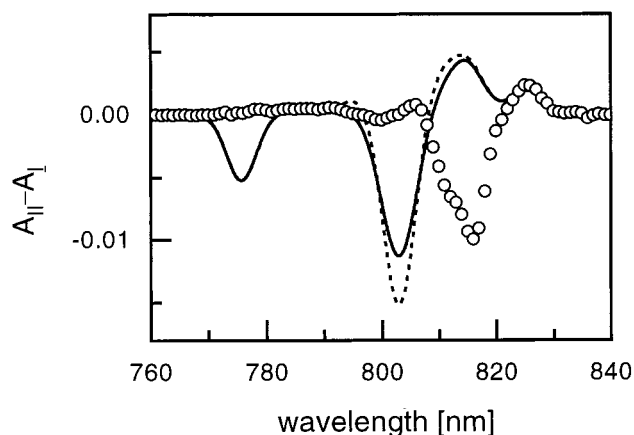


**Figure 8.** Experimental (thick solid line) and simulated (solid, dashed lines) LD spectrum of the FMO complex of *C. tepidum* at 10 K. The spectra were calculated using the parameters as described in ref 25, with (thin solid line) and without (dashed line) including homogeneous broadening.

femtoseconds and one around a few picoseconds, roughly with equal amplitudes, independent of the model used. This result is in better agreement with the measured kinetic data (see Figure 7) than the results obtained with either of the two parameter sets for *P. aestuarii* and confirms the suggestion that the 1.7 and 5.5 ps component found in kinetic measurements[8] should be attributed to energy relaxation within the subunit. Actually, including static disorder results in a situation which is intermediate between the models of *P. aestuarii* summarized in Table 3. Static disorder should of course also affect the simulation for *C. tepidum*, especially for the states containing BChl 5 and/or 6, since they were taken to have equal site energies. However, the lifetimes of states 4 and 6, that have a high contribution of BChls 5 and 6, were already very short so that it was difficult to establish a clear effect of disorder in our simulation. For both species, the optical spectra that were obtained by the Monte Carlo simulation are very similar to those based on the Gaussian dressed stick spectra published earlier.[1,2] For this reason, we have focused on the latter approach in a consistent effort to keep the model as simple as possible.

Recently Renger and May[25] simulated the absorption and time-resolved absorbance difference spectra for the FMO complex of *C. tepidum* by a method that took into account effects of diagonal disorder and homogeneous broadening, using a dipole strength of 51 D[2]. To test the validity of their model, we have calculated absorption, LD, CD, and T−S spectra and compared those with experimental[2] data. The CD spectrum could be well described, but the T−S and LD spectra did not fit at all; the prominent negative peak at 816 nm in the experimental LD spectrum was located at 803 nm in the simulated spectrum (Figure 8). The simulated LD as well as the simulated absorption spectrum showed a conspicuous band at 775 nm, not present in the experimental data. Especially the LD spectrum is important, since it contains essential information about the orientation of the transition dipoles of the system and is a sensitive indication for the validity of the simulation as was discussed previously by Gülen.[5] Also, the simulated absorbance difference spectrum of the lowest exciton state (state 1) did not fit the measured ones at longer delay. Therefore, we conclude that the parameters used by Renger and May[25] for describing the electronic structure of *C. tepidum* are not appropriate, although their sophisticated method for describing the spectral broadening may in the future lead to an improvement of the details of the simulated spectra.

Excited State Dynamics in FMO Antenna Complexes

*J. Phys. Chem. B, Vol. 103, No. 38, 1999* **8161**

BChl *a* in solution has an excited-state absorption (S$_1 \rightarrow$ S$_n$),[45] which at room temperature is a very broad band with significant oscillator strength and a width of at least 300 nm. Some groups[25,46] have taken this intramolecular excited state absorption into account in the simulations and showed a large effect of the dipole strength of the S$_1 \rightarrow$ S$_n$ transitions on the results of the calculations. Our simulations provide a sensitive test for the effect of the intramolecular excited state absorption. As shown previously,[7] the absorbance difference spectra for the various exciton states are the differences between the simulated excited state spectra on one hand and the ground state and stimulated emission spectra on the other and therefore are very sensitive indicators for the validity of the simulation. The difference spectrum of state 1 as well as the spectra of mixtures of other states showed excellent agreement with the measured spectra.[7] An almost perfect match was also obtained with the spectra measured by Freiberg et al.[14] This shows that the contribution from intramolecular excited state absorption is not significant and does not affect our simulations, as was also suggested by Savikhin et al.[47] We conclude that the reported spectrum of intramolecular excited state absorption[45] of BChl *a* in solution at room temperature does not apply to BChl *a* in the FMO complex at low temperature.

It is likely that specific vibrations, both from the protein and the BChl molecules themselves, play an important role in the relaxation processes. Especially when the energy difference between two states coincides with that of a specific vibrational band, relaxation between those exciton states could be accelerated by enhanced vibrational coupling. Vibrations have been observed by resonance Raman spectroscopy,[48] and the discrepancy between $\gamma(\omega)$ and the fluorescence spectrum of Figure 1, that can be seen around 190 cm$^{-1}$, possibly can be attributed to a vibrational band. Renger and May[25] have accounted for protein vibrations by including a so-called correlation radius of the exciton vibrational interaction in the description of the spectral density in their model. Since the exact energies and the strength of the electron−phonon coupling are unknown for both the protein vibrations and the intramolecular vibrations of BChl *a* in the FMO complex, we used a function $\gamma(\omega)$ as described by eq 6 to describe the overall vibronic coupling to the exciton states.

We conclude that our exciton model for the FMO complex of *C. tepidum* describes remarkably well both the optical steady-state spectra and the dynamics of the excited state. The exciton states preferably relax stepwise downhill through the exciton manifold. The rate constants for the excited state relaxation processes are quite sensitive to the choice of site energies, as demonstrated by the effect of static disorder on the dynamics for the FMO complex of *P. aestuarii*. Generally, however, also for *P. aestuarii* our simulations give a realistic description of the excited-state properties. We have arrived at a consistent model for the FMO complex which has established that the point-dipole approximation is valid, that the electronic structure is determined by intermolecular interaction of BChls with varying site energies, and that the excited state dynamics is governed by linear electron−phonon coupling.

**References and Notes**

(1) Louwe, R. J. W.; Vrieze, J.; Hoff, A. J.; Aartsma, T. J. *J. Phys. Chem. B* **1997**, *101,* 11280.

(2) Vulto, S. I. E.; de Baat, M. A.; Louwe, R. J. W.; Permentier, H. P.; Neef, T.; Miller, M.; van Amerongen, H.; Aartsma, T. J. *J. Phys. Chem. B* **1998**, *102,* 9577.

(3) Pearlstein, R. M. *Photosynth. Res.* **1992**, *31,* 213.

(4) Lu, X.; Pearlstein, R. M. *Photochem. Photobiol.* **1993**, *57,* 86.

(5) Gülen, D. *J. Phys. Chem.* **1996**, *100*, 17683.

(6) Fenna, R. E.; Matthews, B. W. *Nature* **1975**, *258,* 573.

(7) Vulto, S. I. E.; Neerken, S.; Louwe, R. J. W.; de Baat, M. A.; Amesz, J.; Aartsma, T. J. *J. Phys. Chem. B* **1998**, *102,* 10630.

(8) Vulto, S. I. E.; Streltsov, A. M.; Aartsma, T. J. *J. Phys. Chem. B* **1997**, *101,* 4845.

(9) Buck, D. R.; Savikhin, S.; Struve, W. S. *Biophys. J.* **1997**, *72,* 24.

(10) Louwe, R. J. W.; Aartsma, T. J. *J. Lumin.* **1994**, *58,* 154.

(11) Louwe, R. J. W.; Vrieze, J.; Aartsma, T. J.; Hoff, A. J. *J. Phys. Chem. B* **1997**, *101,* 11273.

(12) Savikhin, S.; Struve, W. S. *Photosynth. Res.* **1996**, *48,* 271.

(13) Savikhin, S.; Buck, D. R.; Struve, W. S. *Biophys. J.* **1997**, *73,* 2090.

(14) Freiberg, A.; Lin, S.; Timpmann, K.; Blankenship, R. E. *J. Phys. Chem. B* **1997**, *101,* 7211.

(15) Gulbinas, V.; Valkunas, L.; Kuciauskas, D.; Katilius, E.; Liuolia, V.; Zhou, W.; Blankenship, R. E. *J. Phys. Chem.* **1996**, *100,* 17950.

(16) Johnson, S. G.; Small, G. J. *Chem. Phys. Lett.* **1989**, *155,* 371.

(17) Johnson, S. G.; Small, G. J. *J. Phys. Chem.* **1991**, *95,* 471.

(18) Franken, E. M.; Neerken, S.; Louwe, R. J. W.; Amesz, J.; Aartsma, T. J. *Biochemistry* **1998**, *37,* 5046.

(19) Savikhin, S.; Zhu, Y.; Blankenship, R. E.; Struve, W. S. *J. Phys. Chem.* **1996,** *100,* 3320.

(20) Kenkre, V. M. In *Exciton Dynamics in Molecular Crystals and Aggregates*; Kenkre, V. M., Reineker, P., Eds.; Springer-Verlag: Berlin, 1982.

(21) Kuhn, O.; Renger, T.; May, V.; Voigt, J.; Pullerits, T.; Sundström, V. *Trends Photochem. Photobiol.* **1997**, *4,* 213.

(22) Davydov, A. S. *Theory of Molecular Excitons*; McGraw-Hill Book Company: New York, 1962.

(23) Leegwater, J. A.; Durrant, J. R.; Klug, D. R. *J. Phys. Chem. B* **1997**, *101,* 7205.

(24) Kühn, O.; Sundström, V. *J. Phys. Chem. B* **1997**, *101,* 3432.

(25) Renger, T.; May, V. *J. Phys. Chem. A* **1998**, *102,* 4381.

(26) Francke, C.; Amesz, J. *Photosynth. Res.* **1997**, *52,* 137.

(27) Kennis, J. T. M.; Streltsov, A. M.; Aartsma, T. J.; Nozawa, T.; Amesz, J. *J. Phys. Chem.* **1996**, *100,* 2438.

(28) Kennis, J. T. M.; Streltsov, A. M.; Permentier, H.; Aartsma, T. J.; Amesz, J. *J. Phys. Chem. B* **1997,** *101,* 8369.

(29) Greene, B. J.; Farrow, R. C. *J. Chem. Phys.* **1983**, *98,* 273.

(30) Kennis, J. T. M.; Shkuropatov, A. Y.; van Stokkum, I. H. M.; Gast, P.; Hoff, A. J.; Shuvalov, V. A.; Aartsma, T. J. *Biochemistry* **1997**, *36,* 16231.

(31) van Noort, P. I. Thesis Leiden University, The Netherlands, 1994.

(32) van Amerongen, H.; Struve, W. S. *J. Phys. Chem.* **1991**, *95,* 9020.

(33) Reineker, P. In *Exciton Dynamics in Molecular Crystals and Aggregates*; Kenkre, V. M., Reineker, P., Eds.; Springer-Verlag: Berlin, 1982.

(34) Knox, R. S.; Gülen, D. *Photochem. Photobiol.* **1993**, *57,* 40.

(35) Rahman, T. S.; Knox, R. S.; Kenkre, V. M. *Chem. Phys.* **1979**, *44,* 197.

(36) Savikhin, S.; Buck, D. R.; Struve, W. S. *Chem. Phys.* **1997**, *223,* 303.

(37) Louwe, R. J. W.; Aartsma, T. J. *J. Phys. Chem.* **1997**, *101,* 7221.

(38) Blum, K. *Density Matrix Theory and Applications*; Plenum Press: New York, 1981.

(39) Tronrud, D. E.; Schmid, M. F.; Matthews, B. W. *J. Mol. Biol.* **1986**, *188,* 443.

(40) Li, Y. F.; Zhou, W.; Blankenship, R. E.; Allen, J. P. *J. Mol. Biol.* **1997**, *271,* 456.

(41) Pullerits, T.; Monshouwer, R.; van Mourik, F.; van Grondelle, R. *Chem. Phys.* **1995,** *194,* 395.

(42) Kolaczkowski, S. V.; Hayes, J. M.; Small, G. J. *J. Phys. Chem.* **1994**, *98,* 13418.

(43) Jankowiak, R.; Hayes, J. M.; Small, G. J. *Chem. Rev.* **1993**, *93,* 1471.

(44) Fidder, H.; Knoester, J.; Wiersma, D. A. *J. Chem. Phys.* **1991**, *95,* 7880.

(45) Becker, M.; Nagarajan, V.; Parson, W. W. *J. Am. Chem. Soc.* **1991**, *113,* 6840.

(46) Pullerits, T.; Chachisvilis, M.; Sundström, V. *J. Phys. Chem.* **1996**, *100,* 10787.

(47) Savikhin, S.; Buck, D. R.; Struve, W. S. *J. Phys. Chem. B* **1998**, *102,* 5556.

(48) Lutz, M.; Hoff, A. J.; Brehamet, L. *Biochim. Biophys. Acta* **1982**, *679,* 331.